Adipocyte size distribution: Mathematical model of a tissue property

Aloïs Dauger, Hedi Soula, Chloe Audebert

Mathematical Biosciences 384 (2025) 109433

Contents lists available at ScienceDirect

Mathematical Biosciences

journal homepage: www.elsevier.com/locate/mbs

Original Research Article

Adipocyte size distribution: Mathematical model of a tissue property

Aloïs Dauger [a,b,*], Hedi Soula [a], Chloe Audebert [b,c]

[a] Sorbonne Université, Inserm, Nutrition and obesities: systemic approaches, Nutriomics, F-75013, Paris, France
[b] Sorbonne Université, Université Paris Cité, CNRS, Laboratoire Jacques-Louis Lions, LJLL, F-75005, Paris, France
[c] Sorbonne Université, CNRS, Laboratoire de Biologie Computationnelle, Quantitative et synthétique, CQSB, F-75005, Paris, France

ARTICLE INFO

MSC:
92C30
92C35

Keywords:
Obesity
Adipocytes
Size distribution
Cell variability

ABSTRACT

White adipose tissue is in charge of storing excess of energy in form of lipids. The main cells involved in the process – the adipocytes – adapt their sizes up to 200 μm of diameter to accommodate the storage. In addition, their size distribution is bimodal. A previous mathematical model based on lipid fluxes provided size distribution bimodality. However, the variability within cell population was not fully explored. In the previous model, bimodality was considered a consequence of a bistable distribution of cell sizes at equilibrium: meaning that adipocytes had to have two stable sizes. In this study, we first provide a computational method to evaluate equilibria taking into account cells variability. Our results suggest that this variability is key to provide realistic distributions. In addition, we show that size distributions with a proportion of cell with bi-stable profile are not in good agreement with the measurements. We find that mono-stable (i.e. one equilibrium size) profile within the adipose tissue is enough to explain bimodality and to reproduce qualitatively size distribution data. We thus show that bimodality of adipose tissue size distribution does not arise directly from cellular bi-stability but rather from a tissue property.

0. Introduction

Obesity is one of the main public health issue. Its magnitude makes it a global problem as its worldwide prevalence is about 14% [1]. Also, it is estimated to have engendered about 5 millions premature deaths in 2017 [2]. Not only can obesity cause various metabolic diseases, but it is a comorbidity as sadly illustrated during the COVID-19 pandemic: 70%–90% of patients who were admitted to the Intensive Care Units (ICU) were overweight [3,4]. Thus, understanding the underlying mechanisms of obesity is an urgent current research challenge.

White Adipose Tissue (WAT) is central in obesity emergence and sustain as it is in charge of storing lipids. Adipocytes, its main constitutive cells, can store lipids by increasing either in size (hypertrophy) or in number (hyperplasia). Adipocytes are able to deflate via lipolysis (i.e. lipids release) or inflate via lipogenesis (i.e. lipids entry). The size of these cells is known to be linked to tissue and systemic dysfunctions. An adipose tissue composed of large adipocytes is more likely to be subject to tissue hypoxia, low-grade inflammation, senescence, fibrosis and insulin resistance [5]. All these processes may lead to obesity-related pathologies. The WAT shows interesting diversity properties: not only adipocytes have a vast size range going from 15 μm to 200 μm of diameter, but the size distribution is bimodal. The underlying mechanisms of this uncommon cellularity remain poorly understood. The size distribution is also specie and subject dependant but the bimodal shape is conserved as shown in Fig. 1. As a result, neither the adipocytes can be summarized by one characteristic size within a subject (as the size distribution is not unimodal), nor a distribution can summarize the sizes within a specie (as they differ depending on the individual condition - e.g. lean vs obese). This makes the adipose cell size distribution a personal physiological feature, that may be crucially informative regarding metabolic health or proneness to develop obesity-associated disease [6].

The origin of the bimodality is unclear as the mechanisms leading to it remains misunderstood. In order to reproduce it, a few mathematical models have emerged [7,8]. These models succeed in reproducing adipose cells size distributions but the parameters are lacking of biological meaning. A mechanistic model, based on ordinary differential equations, with more interpretable terms was published by H.Soula and his colleagues [9,10]. More recently, a derived model, based on partial differential equations, has been proposed [11]. This latter model includes a constant diffusion term which is difficult to link to an explicit physiological process. A different approach has also been proposed recently with a Lifshitz–Slyozov type model, based on a transport partial differential equation, for the dynamics of the size distribution of adipose cells [12].

The objective of this article is to study equilibria of the model proposed in [9], in order to qualitatively reproduce size distributions

* Corresponding author.
E-mail address: alois.dauger@sorbonne-universite.fr (A. Dauger).

https://doi.org/10.1016/j.mbs.2025.109433
Received 10 September 2024; Received in revised form 30 January 2025; Accepted 20 March 2025
Available online 9 April 2025

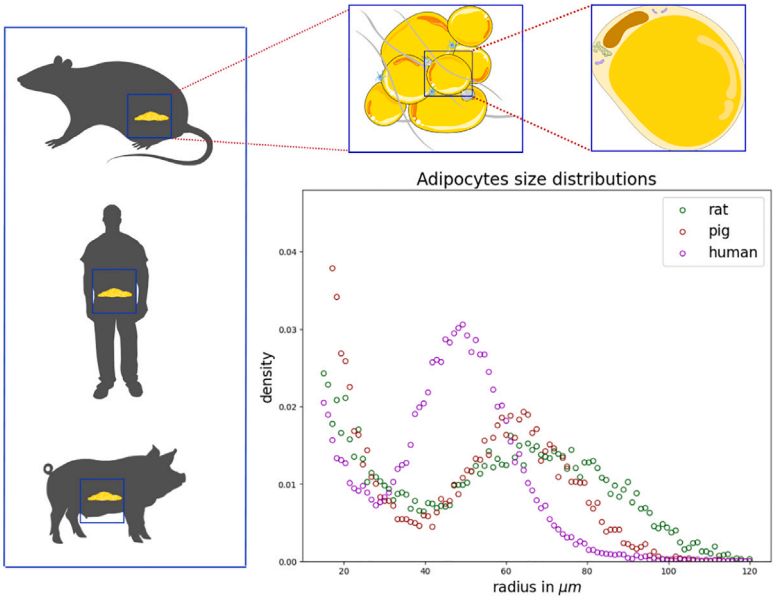

Fig. 1. The size distributions of adipocytes collected in rat (green), mini-pig (red) and human (magenta) are displayed on the bottom-right panel for illustrative purpose.

measured in rat, mini-pig and human with an interpretable source of variability. To do so, we introduce an iterative method for computing the steady states of the model proposed in [9]. Then, we show that some intrinsic variability within the cell's dynamic allows to qualitatively reproduce the measured cell size distribution. In doing so, we show that the adequate range of parameters obtained is for mono stable distribution and not for bistable ones. We also reproduce several properties expected for the adipose tissue. Finally we discuss the results in regards of the previous mathematical model that have described adipose cell size distributions.

1. Model and methods

1.1. Adipocyte size distribution measurements

The adipocytes size distributions were obtained by Multisizer 3 Coulter Counter (Beckman Coulter, Brea, CA, USA) after osmium tetroxide fixation as described previously [9,13]. We obtained distribution from previous studies for illustrative purposes from several tissues and several species in published or unpublished material.

1.2. Mathematical model of adipocyte size distribution

The model used in this paper was first proposed by Soula et al. [9]. It is based on ordinary differential equation (ODE) describing the evolution of the lipids content in a cell over time (see Eq. (1)). Assuming that no lipids are created neither disappear, it only depends on lipids uptake *'lipogenesis'* and lipids release *'lipolysis'* (i.e. overall lipid fluxes).

$$\frac{d\ell}{dt} = \underbrace{\alpha r^2 \frac{L}{L+\kappa}\frac{\rho^n}{\rho^n + r^n}}_{lipogenesis} - \underbrace{(\beta + \gamma r^2)\frac{\ell}{\ell + \chi}}_{lipolysis} = f_\theta(r, L), \tag{1}$$

with

$$\ell = V(r) = \frac{4\pi}{3V_\ell}(r^3 - r_0^3).$$

Where ℓ is the amount of lipids stored in the cell (nmol), r is the cell radius (μm). They are directly linked assuming the sphere shape of adipose cell [14], through V_ℓ the molar volume of triglycerides ($\mu m^3.nmol^{-1}$) and r_0 the radius of an empty cell (μm). L is the amount of extra-cellular lipids (nmol). The model parameters are: $\theta = [\alpha, \beta, \gamma, \rho, \kappa, \chi, n]$ (real positive numbers). Both lipogenesis and lipolysis are assumed to be areal fluxes (proportional to the cell surface — assuming a common receptor density) [10,15] respectively weighted by α and γ ($nmol.\mu m^{-2}.h^{-1}$). Following [10], parameter γ models the lipolysis because of Noradrenalin stimulation and the basal lipolysis is taken into account via β term ($nmol.h^{-1}$) since lipid release is also performed by cells without Noradrenalin stimulation. The expansion of the cell is limited by the extra-cellular matrix and surrounding cells pressure, modeled by ρ (μm) via the Hill-like function term $\frac{\rho^n}{\rho^n + r^n}$. The κ and χ parameters (nmol) allow fluxes lowering under limiting conditions via $\frac{L}{L+\kappa}$ and $\frac{\ell}{\ell+\chi}$ terms.

Thus, considering N cells is equivalent to dealing with a system of ODE in which each equation describes the dynamics of a cell, it follows

$$\begin{cases} \frac{d\ell_i}{dt} & = \alpha_i r_i^2 \frac{L}{L+\kappa_i}\frac{\rho_i^n}{\rho_i^n + r_i^n} - (\beta_i + \gamma_i r_i^2)\frac{\ell_i}{\ell_i + \chi_i} = f_{\theta_i}(r_i, L) \text{ for } i \in \{1 \dots N\} \\ L & = \mathcal{L}_{tot} - \sum_{i=1}^{N} \ell_i = \mathcal{L}_{tot} - \sum_{i=1}^{N} V(r_i), \end{cases} \tag{2}$$

where $\mathcal{L}_{tot}$ is a parameter of the system representing the total amount of lipids in nmol (sum of intra- and extra- cellular). In order to include variability within population of cell, we introduce a frozen randomness on the parameters of system (2). The parameters are normally distributed, the mean represents the population parameter, and the variation is described by a coefficient of variation (the relative standard deviation defined by the ratio of standard deviation over mean). In the following, the presented size distributions are simulated with $N = 10^4$ cells.

1.3. Numerical method

In the aim of qualitatively reproducing the measured size distributions, we make the assumption that the system is at equilibrium. This assumption is supported by the constancy of the size distribution when the energy intake matches the energy expenditure [16]. We are thus interested by steady state solutions of system (2). We therefore will not consider the time evolving system but only steady states and we will

solve numerically system (2) at equilibrium:

$$\begin{cases} \dfrac{d\ell_i^*}{dt} = f_{\theta_i}\left(r_i^*, L^*\right) = 0, \\ L^* - \mathcal{L}_{tot} + \displaystyle\sum_{i=1}^{N} V(r_i^*) = 0. \end{cases} \tag{3}$$

To find equilibria we implemented the Brent-Decker method which is a robust numerical technique used to locate the zeros of a function within a specified interval [17]. This method combines elements of bisection, secant, and inverse quadratic interpolation to efficiently converge towards the roots of the function in the initial interval. It iterates to narrow down the interval containing the root of the function and stops when the desired level of accuracy is achieved. To find a solution of system (3) the algorithm starts with two values L_{left} and L_{right} assuming $L^* \in [L_{left}, L_{right}]$. We chose $[0.01, 10 \times N]$ for the initial interval of L, where N is the number of considered cells. In our cases, it ensures the condition $L^* \in [L_{left}, L_{right}]$. We solve $L - \mathcal{L}_{tot} + \sum_{i=1}^{N} V(x_i) = 0$ and stop with level of accuracy 10^{-4} with Brent-Decker algorithm. This method is based on successive evaluations of the function at different points in the initial interval. We define $\phi : L \mapsto L - \mathcal{L}_{tot} + \sum_{i=1}^{N} V(x_i)$, where x_i depends on L and is a solution of $f_{\theta_i}(x_i, L) = 0$. For each evaluation of ϕ, the x_i values are estimated by solving $\tilde{f}_\theta(x, L) = 0$, where $\tilde{f}_\theta(x, L) = (V(x) + \chi) f_\theta(x, L)$. To do so, we evaluate the function $x \mapsto \tilde{f}_\theta(x, L)$ on evenly spaced values in the interval $[5, 150]\,\mu\text{m}$. The sign changes allow us to define intervals containing roots of the function. These intervals are starting points for the Brent-Decker method that stops with accuracy 10^{-6}. So, for each function $x \mapsto \tilde{f}_{\theta_i}(x, L)$ we find all the zeros between 5 μm and 150 μm.

In the range of parameters that we consider in this work, the functions $x \mapsto f_{\theta_i}(x, L)$ have either one or three zeros. From the sign of f_θ we then identify either one stable zero (local flow is towards it) or two stable and one unstable (local flow is away from it) zeros. For each f_{θ_i}, if more than one zero are found, we decide to attribute to x_i the value of the largest stable zero. Once Brent-Decker algorithm has converged to an approximation of L^* we can compute the corresponding r_i^* for $i \in \{1 \dots N\}$ solution of system (3). The described method allows us to reach one of the steady states of system (2).

In the following, we will denote as "mono-stable" a cell which parameters lead to a unique stable zero for function f_θ and "bi-stable" the cell for which the function has two stable zeros. With the described approach, the $N + 1$ dimensional problem (3) is now $N + 1$ times a one dimensional problem, that is solved with Brent-Decker method. At the end of the algorithm we obtain an approximation for L^* and r_i^* for $i \in \{1 \dots N\}$ solution of system (3).

This method is implemented in Python and the code is available on Git repository: https://plmlab.math.cnrs.fr/aloisdauger/adipocytes_modeling.

1.4. Model simplification: extra-cellular lipids are constant

In order to simplify the solution computation and therefore enable parameter space exploration, we consider that all the equations of system (1) are decoupled and L become a parameter of the system. This simplification can be seen as a change in the considered parameter for lipids amount. Indeed, initially the total amount of lipids in the system was the parameter of interest : $\mathcal{L}_{tot}$. Now, the parameter of interest is the amount of extra-cellular lipids L, with this modification we assume all the adipocytes have access to a constant amount of lipids within the blood and do not impact this constant. Now L is a parameter, so the steady state solution is computed with Brent-Decker method as described before by approximating the roots between 5 μm and 150 μm of all functions $x \mapsto f_{\theta_i}(x, L)$, $i \in \{1 \dots N\}$.

In this work, we have two competing hypothesis to explain the bimodal distribution of the adipocytes size distribution. Hypothesis 1: the cell radius has two stable states explaining the two characteristic sizes observed in the population of cells. Hypothesis 2: the cell radius has a unique stable state that varies largely in the population of cell due to inter-cell variability. Here, we propose an approach to identify the most plausible hypothesis.

Table 1
Range of values for the exploration of parameters' space. First column recalls parameters name of system (2), second column displays the considered parameter range and the last column give the number of tested values within this range.

Range of parameters explored			
	range	# tested values	units
α	[0.2, 0.5]	20	nmol μm^2 h^{-1}
β	[0, 200]	11	nmol h^{-1}
γ	[0.001, 0.1]	10	nmol μm^2 h^{-1}
χ	[0.1, 0.5]	10	nmol
L	[0.05, 0.5]	5	nmol

We considered relatively large range of values for the following parameters: $\alpha, \beta, \gamma, \chi, L$. We fixed intervals bounds for each parameter based on previous estimations [10,11]. The ranges chosen to explore the parameters' space are presented in Table 1. This choice leads to 110 000 different combinations of parameters. For each, we evaluate the corresponding function f_θ and we select the θ for which f_θ has 3 zeros in the radii interval $[5, 150]$ (two stable zeros). The selected parameters combinations are prone to engender distributions made of bi-stable cells. For each selected combination of parameters, a distribution is then computed using the numerical method described in Section 1.3 with $N = 5000$ cells and a coefficient of variation of 20% on the 5 considered parameters. As described previously, all bi-stable cells are considered on their larger stable radius.

2. Results

2.1. Intra-cellular variability

For a given set of parameters θ, identical for every cells, the system (2) consists of N identical ODE with identical equilibria for cells. As mentioned in the methods section, we detailed the results when parameters are distributed.

For example if we consider that all the simulated cells differ slightly in their capacity to perform lipid uptake – α. Biologically, it could correspond to different epigenetic states from one cell to another as observed in single cell RNA analysis [18].

The right panels of Fig. 2 display the size distributions obtained by simulating $N = 10^4$ cells with $\alpha \sim \mathcal{N}(\mu = 0.31, \sigma = 0.031)$ across these N cells. Total lipid is fixed at $2.5732\,10^4$ nmol, Table A.2 gives the other parameters for this simulation. Two illustrating cases are shown with two different values of parameter β (corresponding to basal lypolysis): 125 nmol.h^{-1} (Fig. 2A) and 10 nmol.h^{-1} (Fig. 2B). Our numerical method converges in 14 iterations (7.2 s on Macbook Air 2022, under Apple M2 CPU, 24 Gb of RAM). Fig. A.7 shows the numerical convergence of L with respect to iterations as well as the corresponding ϕ function for the two sets of parameters. In Fig. 2A, cells are almost all bi-stable (for 83% of cells, f_θ has 3 zeros) whereas in Fig. 2B are all mono-stable (f_θ has only one zero). Right panels are the resulting distributions and left panels show the corresponding f_θ functions.

With the chosen parameters, a large value for β leads to a majority of bi-stable profiles (Fig. 2 A). In this case, we consider all bi-stable cells on their larger stable zero. Thus, the left mode is composed of mono-stable cells only. The distribution obtained is indeed bimodal but lacks other features. The left mode has no variability and the size distribution does not exhibit a continuum in sizes: no cell with radius between 6 μm and 60 μm. The unstable fixed point might be the cause for this absence of intermediate size cells as we can see on the left panel.

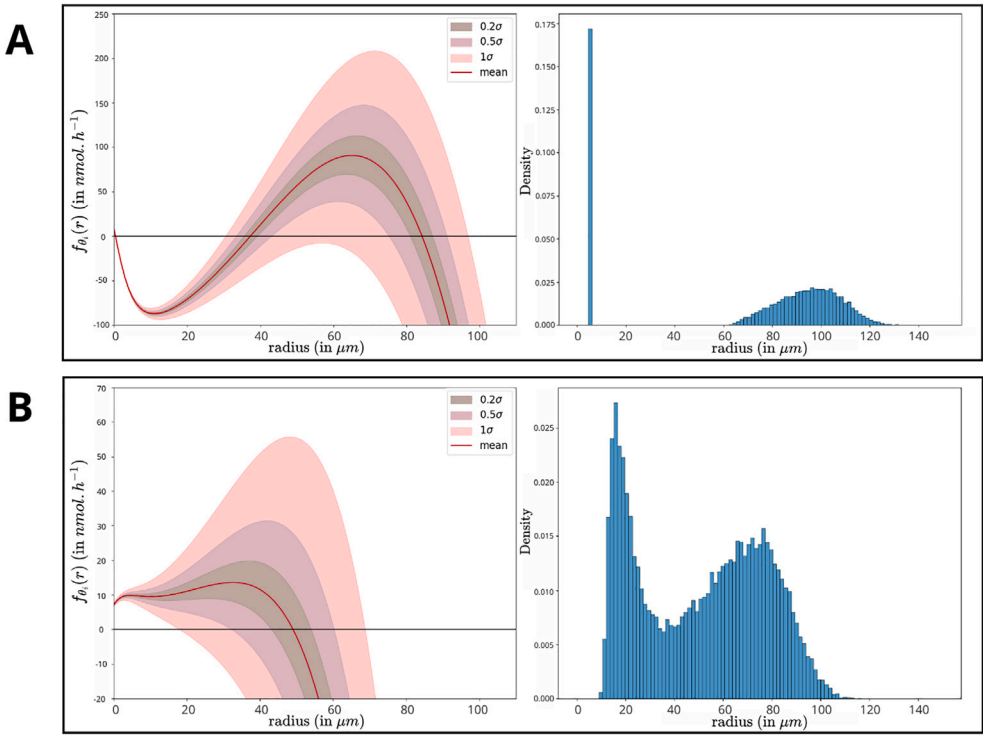

Fig. 2. Distribution obtained with the numerical method described in Section 1.3. On the left the function $r \mapsto f_\theta(r, L)$ is displayed, and the effect of the distribution of parameter α is showed with different amplitudes ($0.2, 0.5$ and 1 σ). On the right, the corresponding size distributions are displayed. **(A)** In simulation A, parameter β is set to 125 nmol.h^{-1}. We observe mostly bi-stable cases, 83% of cells have two stable zeros. To compute the size distribution, the bi-stable cells are set to the larger stable fixed point, all of them constitute the right mode of the distribution. **(B)** In simulation B, we set $\beta = 10$ nmol.h^{-1}, then all cell are mono-stable, and have only one stable zero.

On the other hand, smaller value of β leads to mono-stable profiles (Fig. 2 B) but even if each cell has a unique stable size, cell population still displays a bimodal size distribution. In this case, it results in a more realistic size distribution, with a continuum in sizes qualitatively close to the measured size distribution (Fig. 1) using a coefficient of variation of 10% on a single parameter.

2.2. Bi-stable profiles fail to explain the continuum of sizes observed in adipose tissue

As shown in the previous Section 2.1 our results suggest that range of parameters yielding more than one zero could not provide realistic distribution with our method.

We selected bi-stable parameters profiles according to the protocol outlined in Section 1.4, and used them to compute size distributions. Among the 110 000 tested combinations of parameters, 7910 were selected (i.e $\approx 7.2\%$ describe a bi-stable profile). These set of values were distributed over a population of 5000 cells with a coefficient of variation of 20%. This protocol pulls all cell sizes together to provide a single distribution (composed of $7910 \times 5000 = 3.955 \times 10^7$ cells), displayed on Fig. 3.

Having up to 20% as coefficient of variations, the overall distribution shows no cell of intermediate size (between 20 µm and 40 µm). In other words: the intermediate size cells may not come from a bi-stable profile. Hence, under the assumptions of the proposed model, the mono-stability of the cells appears to be needed to reproduce observed size distributions.

As shown in Fig. 2, an important parameter that governs the number of zeros is β. We compute the zeros of f_θ fixing all parameters to their reference values indicated in Table A.2 except for β and α which vary. The β parameter varies between 0 nmol.h^{-1} to 25 nmol.h^{-1} (interval divided in 150 equal parts) with five different values of α: $\{0.29, 0.3, 0.3045, 0.308, 0.31\}$.

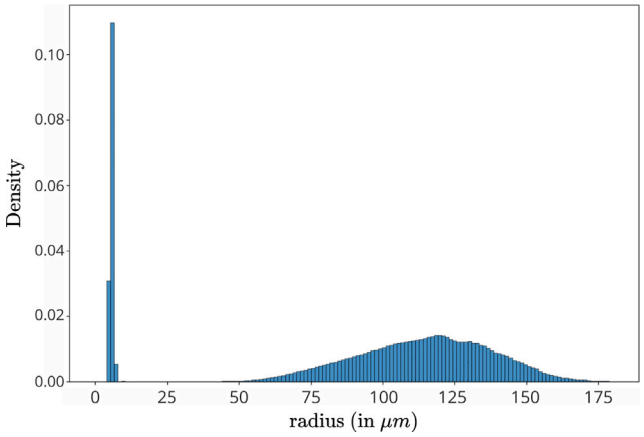

Fig. 3. The cumulative histogram of cells with parameters combination leading to bi-stable profile (see Table 1). The size distributions are computed using the numerical method described in Section 1.3 where L is considered as a parameter. The histogram summaries $7910 \times 5000 = 3.955 \times 10^7$ cell sizes for different parameter combinations.

For the tested values, on Fig. 4 we observe a cusp bifurcation with respect to α and β parameters. Unlike supercritical pitchfork bifurcation, we do not observe symmetry between the two stable fixed points with respect to the unstable one. The cusp bifurcation is an imperfect bifurcation: it is characterized by the emergence of a gap between the two stable fixed points.

Therefore, it exist a couple of value (α^*, β^*) at which the bifurcation occurs. A value of $\beta < \beta^*$ leads to a population of mono-stable cells. Otherwise, for $\beta \geqslant \beta^*$, distributing α over the population can lead to a population with mixed stability profiles (cells assigned an $\alpha \geqslant \alpha^*$ are bi-stable, and cells assigned an $\alpha < \alpha^*$ are mono-stable).

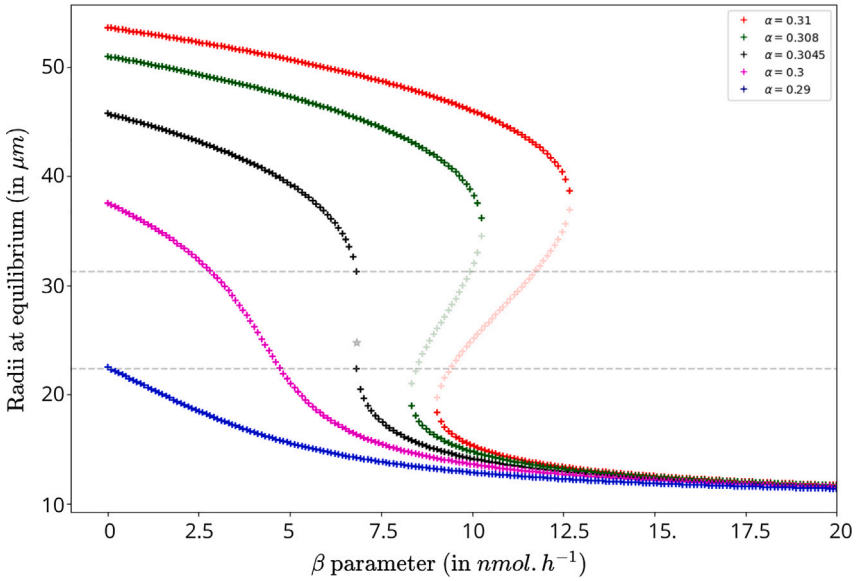

Fig. 4. The zeros of $r \mapsto f_\beta(r, L)$ are computed using the numerical method described in Section 1.3 with respect to β value, for different values of parameter α. The stable zeros are displayed in opaque whereas the unstable ones are transparent. With these parameters and discretization, the curve of $\alpha = 0.3045$ (black crosses) has only one bi-stable cell for $\beta = 7.2$ (parameters close to the cusp point). The black stars highlights its unstable size, whereas the two gray dotted lines [22.4 μm, 31.3 μm] shows the two stable sizes of this cell. This interval approximates the size space beyond the reach of bi-stable profile cells. All other things being equal, there is no couple of values for α, β that allows a stable size within this interval.

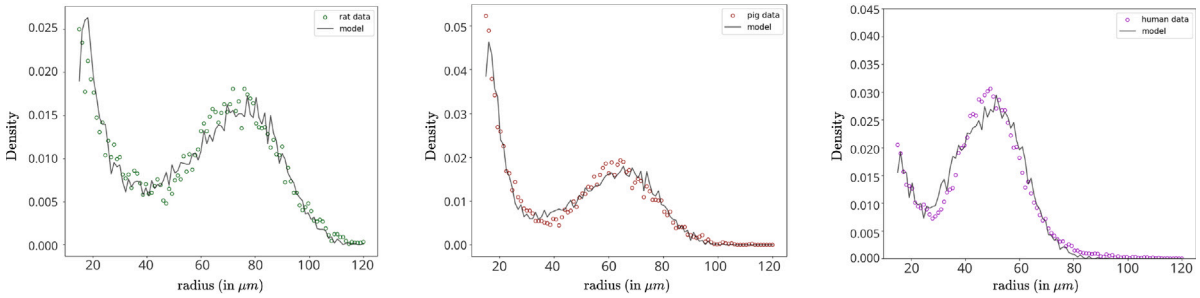

Fig. 5. Qualitative reproduction of data. Data are size distributions measured -from left to right- in: rat (green dots), mini-pig (red dots) and human (magenta dots). The model is displayed in black lines in each panel. The parameter of each are summed up in Table A.3. Their values were obtained by manually tuning a few parameters, considering that external lipids are constant as described in Section 1.4.

Due to this cusp bifurcation, the bi-stable profiles show no stable zero on intermediate sizes (between 22.4 μm and 31.3 μm as shown by the dotted gray lines in Fig. 4). Hence, mono-stable cells are essential to obtain intermediate sizes cell and so realistic size distributions.

2.3. The proposed model qualitatively reproduces adipocyte size distributions of different species

Using the numerical method presented in Section 1.3 we can quickly compute steady states. By manually adjusting a few key parameters, and only distributing α within the cell population with a coefficient of variation of 12%, we qualitatively reproduced adipocyte size distributions of a rat, a mini-pig and a human. Results are presented in Fig. 5.

The proposed model qualitatively reproduces the measured size distributions. In particular, the model matches the distributions' nadir, right mode position, thickness and height. In addition, it presents a continuum in cell sizes.

However, the smallest cells' sizes (left part of the left mode) are not as well captured. This may be due to noise in data: sizes measured under 20 μm of diameter are not exclusively adipocytes. Since the entire adipose tissue is measured, the smallest size could correspond to immune cells or endothelial vascular cells present in the tissue sample.

This qualitative reproduction of experimental data involves only cells with mono-stable profile. It shows our model ability to capture the essential features of adipocytes size distribution in three different species.

2.4. Maximal storage capacity of adipose tissue

In the presented model, the adipose tissue is at equilibrium. Here, we propose to mimic different equilibrium situations that could be reach after different energy imbalance episodes.

With the intention of exploring our model properties, we considered a decoupled population of adipocyte (L is a parameter of the system). The parameters are fixed to their reference values from Table A.2, with $\beta = 1$ nmol.h^{-1}. Different equilibrium size distributions are computed changing the value of L and the average of α that is the only parameter distributed within the cell population (10% of CV). Fig. 6 shows the obtained size distribution for one value of α as well as the intra-cellular lipids amount with respect to extra-cellular lipids per cell for different values of α.

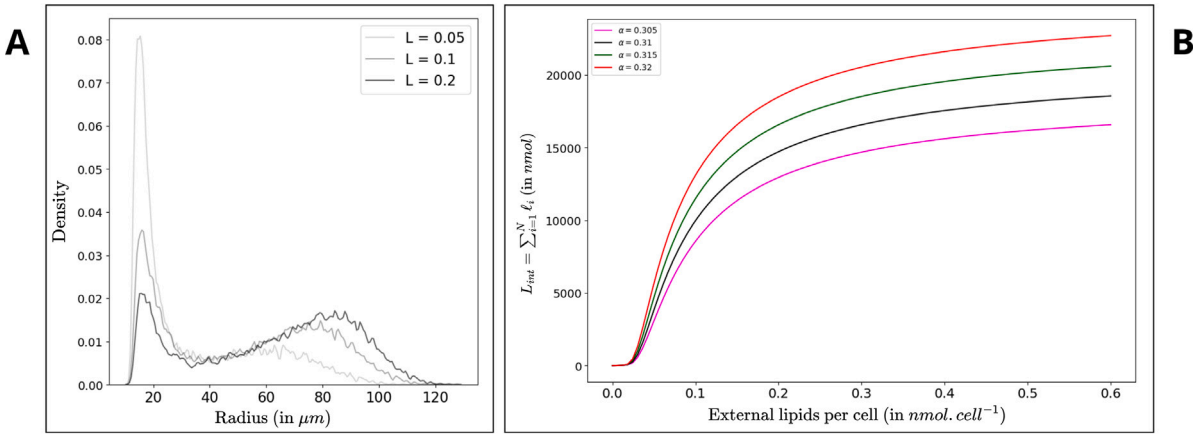

Fig. 6. Effect of extra-cellular lipids on distributions and internal lipids **(A)** Distributions computed for $L \in \{0.05N, 0.1N, 0.2N\}$ and $\alpha \sim \mathcal{N}(\mu = 0.31, \sigma = 0.031)$. **(B)** The internal lipids (the sum of all the lipids carried in cells) versus the extra-cellular lipids per cell for different average value of α in the cell population: 0.305 (magenta), 0.31 (black), 0.315 (green), 0.32 (red).

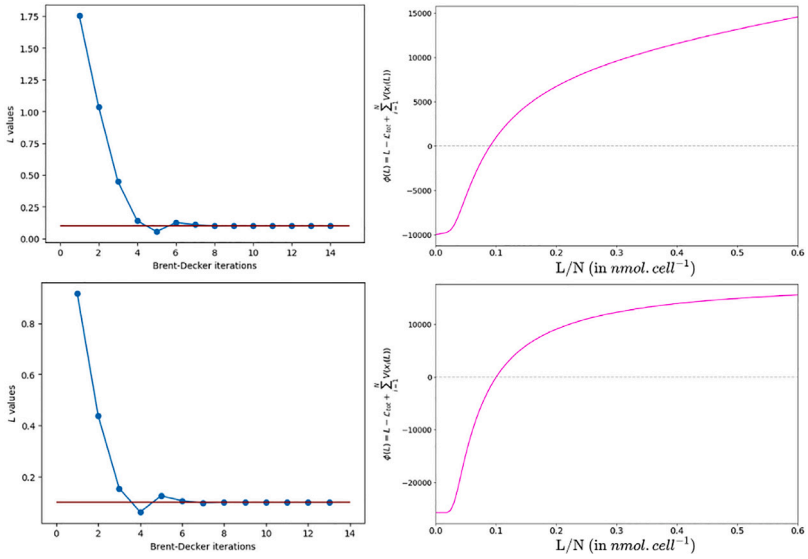

Fig. A.7. Convergence of numerical method for the two considered sets of parameters. The left panels show L values with respect to iterations, the final value approximating L^* is plotted as red line. The right panels show the corresponding curve of the function $\phi : L \mapsto L - \mathcal{L}_{tot} + \sum_{i=1}^{N} V(x_i(L))$. Total lipid $\mathcal{L}_{tot} = 2.5732\,10^4$ nmol, Table A.2 gives the other parameters. The upper panels show the case $\beta = 125$ nmol.h^{-1} (bi-stable case, Fig. 2 A) and the bottom panels show the case $\beta = 10$nmol.h^{-1} (mono-stable case, Fig. 2 B).

Increasing the external lipid amount per cell leads to a shift of the right mode of the distribution: larger cells get even larger. The relative sizes of the two modes are changed: the number of larger cells increases while the number of small cells decreases. The magnitude of this effect depends on α mean values. However, it is limited by the κ parameter: because $L \gg \kappa$ leads to $\frac{L}{L+\kappa} \approx 1$. This implies that the tissue presents a maximum storage capacity beyond which the lipids stay in the extra-cellular compartment (as shown by the plateau on the right panel curves in Fig. 6). Physiologically, in this case, lipids may accumulate in other fat pads or tissues like the liver or muscles, which describes a pathological condition known as dyslipidemia [19].

Furthermore, this maximum storage capacity depends on α. Then, distributing this parameter over the cell population allows more tissue plasticity: some cells are able to inflate more in response to an increase of blood lipids. This may modify the threshold beyond which dyslipidemia is triggered. However, adding lipids in the system always leads to a saturation of the tissue, which supports the need of adipogenesis to store the excess of lipids.

3. Discussion

Understanding the structural properties and size distribution of white adipose tissue is fundamental to unraveling its physiological significance and potential implications in metabolic disorders. Adipocyte size is a crucial feature linked to metabolic health [5,20], but yet we do not understand the underlying mechanisms governing their bimodal size distribution.

In this paper, we aimed to provide a simple numerical solution of the model first published by H. Soula et al. [9] in order to reproduce actual data. In [9], the method was an individual based model with two distributed parameters that was extremely costly to simulate. The method we proposed here computes steady states of the system using Brent-Decker algorithm. The small computational cost allowed us to better understand the effect of the different parameters of the model on size distributions and to highlight the following interesting properties.

We first showed that varying a single parameter over the cell population was sufficient to obtain realistic size distribution. Distributing

the parameters constitute a relevant source of variability that can be interpreted as epigenetic state differences, as observed in [18] where single cell RNA sequencing revealed heterogeneity in cell's lipid uptake ability. The proposed model is deterministic, and with a stochastic model the results presented here could be different. However, from preliminary results (not shown) adding a Brownian motion to the equation does not permit a good agreement between the model and the measurements. We hypothesize that a stochastic model with a noise that depend on cell size could be an interesting model to investigate in order to explain the observed variability in adipose tissue. Instead, we proposed a frozen randomness of one of the parameter (α) of the system following a Gaussian distribution. Other types of variability within adipose tissue could be also explored assuming other distribution for this or other parameters. Here, parameter α represents a complex process involving several actors and pathways, we assumed that such process at the tissue scale can be modeled with a normal distribution.

We showed that we can obtain bimodal distributions made of mono-stable cells: the two modes do not necessarily result from an individual cell property, but can emerge at the tissue scale. With the considered model and in the explored range of parameters we showed that size distributions with a proportion of cell with bi-stable profile are not in good agreement with the measurements. By this exploration of the parameters space and noting a cusp bifurcation, our result suggests that mono-stable cells size within the adipose tissue is enough to explain bimodality and even reproduces qualitatively better the data than in [9] and without relying on diffusion as in [11]. Thereby, bimodality of the adipose tissue size distribution does not seem to arise directly from cellular bi-stability but rather than from a tissue wide property.

We also showed that small differences in particular physiological gene expression can lead to widely different phenotypical – here size – differences. Our findings support the notion that intrinsic differences between adipocytes play a pivotal role in size distribution patterns. This suggests that interventions targeting adipocyte function at the cellular level may hold promise for modulating adipose tissue dynamics and potentially mitigating metabolic dysfunction [21].

However, since we only study the steady states, the dynamic of the adipose tissue is not described completely. Indeed, we assumed complete lipid homeostasis where lipids accumulation is the real cause of obesity. We show that to some extend lipid storage can be plastically increased by increasing cell size (hypertrophy). But evidence suggests that cell number can also be modified (hyperplasia). The trade-off between hypertrophy and hyperplasia remains poorly understood. The joint action of these two mechanisms may lead to complex dynamical properties that have not yet been explored with this model. Taking adipogenesis – new cell recruitment – into account in modeling adipose tissue dynamics could lead to the emergence of crucial properties such as hysteresis with respect to lipid accumulation. This may lead to several advancements in understanding the underlying mechanisms of this physiologically central tissue.

CRediT authorship contribution statement

Aloïs Dauger: Writing – original draft, Visualization, Investigation, Formal analysis, Conceptualization. **Hedi Soula:** Writing – review & editing, Supervision, Methodology, Investigation. **Chloe Audebert:** Writing – review & editing, Supervision, Methodology, Investigation.

Declaration of competing interest

The authors declare that they have no known competing financial interests or personal relationships that could have appeared to influence the work reported in this paper.

Acknowledgments

This work was supported by the ANR MATIDY grant (ANR-20-CE45-0003). We would like to express our gratitude to Magali Ribot for her expertise on numerical schemes. We also thank Christophe Soulage and Emmanuelle Canet Soulas for sharing their data.

Table A.2
Units and values of reference for parameters $\gamma, \rho, \kappa, \chi$, and n.

Values of reference for fixed parameters		
parameter	unit	value
γ	nmol μm^{-2} h^{-1}	0.27
ρ	µm	150
κ	nmol	0.01
χ	nmol	0.0011
n	–	3

Table A.3
Values of parameters used to reproduce the measured size distributions in Fig. 5. The value mentioned for α parameter are the mean and standard deviation of its normal distribution.

Values of parameters for data reproduction							
Subject	α	β	γ	ρ	κ	χ	L
Rat	0.307 ± 0.035	1	0.27	145	0.01	0.0018	0.15
Mini-pig	0.298 ± 0.024	4	0.27	145	0.01	0.0016	0.16
Human	0.29 ± 0.029	4	0.24	88	0.01	0.0015	0.18

Appendix

A.1. Reference parameters

See Table A.2.

A.2. Parameters for data reproduction

See Table A.3.

A.3. Convergence of the numerical method

See Fig. A.7.

Data availability

A link to the code used in this article is mentioned.

References

[1] K.B. Smith, M.S. Smith, Obesity statistics, Prim. Care: Clin. Off. Pr. 43 (1) (2016) 121–135, http://dx.doi.org/10.1016/j.pop.2015.10.001.
[2] H. Ritchie, M. Roser, Obesity, Our World Data (2017).
[3] J. Lighter, M. Phillips, S. Hochman, S. Sterling, D. Johnson, F. Francois, A. Stachel, Obesity in patients younger than 60 years is a risk factor for COVID-19 hospital admission, Clin. Infect. Dis. 71 (15) (2020) 896–897.
[4] A. Simonnet, M. Chetboun, J. Poissy, V. Raverdy, J. Noulette, A. Duhamel, J. Labreuche, D. Mathieu, F. Pattou, M. Jourdain, LICORN and the Lille COVID-19 and Obesity study group, High prevalence of obesity in severe acute respiratory syndrome coronavirus-2 (SARS-CoV-2) requiring invasive mechanical ventilation, Obes. (Silver Spring) 28 (7) (2020) 1195–1199.
[5] J.R. Acosta, I. Douagi, D.P. Andersson, J. Bäckdahl, M. Rydén, P. Arner, J. Laurencikiene, Increased fat cell size: a major phenotype of subcutaneous white adipose tissue in non-obese individuals with type 2 diabetes, Diabetologia 59 (3) (2016) 560–570, http://dx.doi.org/10.1007/s00125-015-3810-6, URL http://link.springer.com/10.1007/s00125-015-3810-6.
[6] T. Cabeza De Baca, S. Parrington, S. Votruba, P. Piaggi, J. Krakoff, D.C. Chang, Adipocyte size, adipose tissue calories, and circulating adipokines, before and after diet-induced weight loss in humans, Endocrine (2024) http://dx.doi.org/10.1007/s12020-023-03666-3, URL https://link.springer.com/10.1007/s12020-023-03666-3.
[7] J. Jo, O. Gavrilova, S. Pack, W. Jou, S. Mullen, A.E. Sumner, S.W. Cushman, V. Periwal, Hypertrophy and/or hyperplasia: Dynamics of adipose tissue growth, PLoS Comput. Biol. 5 (3) (2009) 1–11, http://dx.doi.org/10.1371/journal.pcbi.1000324.

[8] J. Jo, Z. Shreif, V. Periwal, Quantitative dynamics of adipose cells, Adipocyte 1 (2) (2012) 80–88, http://dx.doi.org/10.4161/adip.19705.

[9] H. Soula, H. Julienne, C. Soulage, A. Géloën, Modelling adipocytes size distribution, J. Theoret. Biol. 332 (2013) 89–95, http://dx.doi.org/10.1016/j.jtbi.2013.04.025.

[10] H. Soula, A. Géloën, C. Soulage, Model of adipose tissue cellularity dynamics during food restriction, J. Theoret. Biol. 364 (2015) 189–196, http://dx.doi.org/10.1016/j.jtbi.2014.08.046.

[11] A.-S. Giacobbi, L. Meyer, M. Ribot, R. Yvinec, H. Soula, C. Audebert, Mathematical modeling of adipocyte size distributions: Identifiability and parameter estimation from rat data, J. Theoret. Biol. 581 (2024) 111747, http://dx.doi.org/10.1016/j.jtbi.2024.111747, URL https://linkinghub.elsevier.com/retrieve/pii/S0022519324000286.

[12] L. Meyer, M. Ribot, R. Yvinec, A Lifshitz–Slyozov type model for adipocyte size dynamics: limit from Becker–Döring system and numerical simulation, J. Math. Biology 88 (2) (2024) 16, http://dx.doi.org/10.1007/s00285-023-02036-x, URL https://hal.inrae.fr/hal-04525358.

[13] E. T.D., T. E.H., A. C.E., Improved techniques for studies of adipocyte cellularity and metabolism., J. Lipid Res. 18 (4) (1977) 552–557.

[14] S.D. Parlee, S.I. Lentz, H. Mori, O.A. MacDougald, Quantifying Size and Number of Adipocytes in Adipose Tissue, in: Methods in Enzymology, vol. 537, Elsevier, 2014, pp. 93–122, http://dx.doi.org/10.1016/B978-0-12-411619-1.00006-9, URL https://linkinghub.elsevier.com/retrieve/pii/B9780124116191000069.

[15] A. Moody, M. Stan, M. Stan, J. Gliemann, A simple free fat cell bioassay for insulin, Horm. Metab. Res. 6 (01) (1974) 12–16, http://dx.doi.org/10.1055/s-0028-1093895.

[16] E.D. Rosen, B.M. Spiegelman, Adipocytes as regulators of energy balance and glucose homeostasis, Nature 444 (7121) (2006) 847–853.

[17] R.P. Brent, Algorithms for minimization without derivatives, Prentice-Hall series in automatic computation, Prentice-Hall, Englewood Cliffs, N.J, 1972.

[18] R.Z. Ye, E. Montastier, F. Frisch, C. Noll, H. Allard-Chamard, N. Gévry, A. Tchernof, A.C. Carpentier, Adipocyte hypertrophy associates with in vivo postprandial fatty acid metabolism and adipose single-cell transcriptional dynamics, iScience 27 (1) (2024) 108692, http://dx.doi.org/10.1016/j.isci.2023.108692, URL https://linkinghub.elsevier.com/retrieve/pii/S2589004223027694.

[19] N.P.A.O.A.A. Rehman, Dyslipidemia, React. Wkly. 2010 (1) (2024) 337–337, http://dx.doi.org/10.1007/s40278-024-60179-0, URL https://link.springer.com/10.1007/s40278-024-60179-0.

[20] S. Laforest, J. Labrecque, A. Michaud, K. Cianflone, A. Tchernof, Adipocyte size as a determinant of metabolic disease and adipose tissue dysfunction, Crit. Rev. Clin. Lab. Sci. 52 (6) (2015) 301–313.

[21] A. Regmi, E. Aihara, M.E. Christe, G. Varga, T.P. Beyer, X. Ruan, E. Beebe, L.S. O'Farrell, M.A. Bellinger, A.K. Austin, Y. Lin, H. Hu, D.L. Konkol, S. Wojnicki, A.K. Holland, J.L. Friedrich, R.A. Brown, A.S. Estelle, H.S. Badger, G.S. Gaidosh, S. Kooijman, P.C. Rensen, T. Coskun, M.K. Thomas, W. Roell, Tirzepatide modulates the regulation of adipocyte nutrient metabolism through long-acting activation of the GIP receptor, Cell Metab. 36 (7) (2024) 1534–1549.e7, http://dx.doi.org/10.1016/j.cmet.2024.05.010, URL https://linkinghub.elsevier.com/retrieve/pii/S1550413124001864.